ChemComm
Chemical Communications

Accepted Manuscript

This article can be cited before page numbers have been issued, to do this please use: H. Liang, Q. Bi, A. Hu, X. Chen, R. Jin, X. Song, B. Ke, M. Barz and Y. Nie, *Chem. Commun.*, 2020, DOI: 10.1039/C9CC10071G.

ROYAL SOCIETY OF CHEMISTRY

rsc.li/chemcomm

View Article Online
DOI: 10.1039/C9CC10071G

COMMUNICATION

Nitroreductase and glutathione responsive nanoplatform for integration of gene delivery and near-infrared fluorescence imaging

Received 00th January 20xx,
Accepted 00th January 20xx

DOI: 10.1039/x0xx00000x

Hong Liang[a, †], Qunjie Bi[a, †], Ao Hu[a], Xiaobing Chen[a], Rongrong Jin[a], Xu Song[a,b,*], Bowen Ke[a], Matthias Barz[c] and Yu Nie[a, *]

A novel platform rationally integrated indocyanine green analogues and arginine-rich dendritic peptide with both nitroreductase (NTR) and glutathione (GSH) reduction responsive linker was developed. This mutifunctional platform can enable selective and efficient gene delivery and specific turn-on fluorescence imaging in tumor.

Tumor cells, tumor associated cells, cellular and extracellular matrix components constitute an orchestrated "tumor microenvironment", promoting the growth, invasion and metastasis of tumors.[1] A hallmark of solid tumor microenvironment is hypoxia, originating from the insufficient oxygen supply of blood from disorganized vasculature.[2] Hence, the biomarkers of hypoxia, such as the overexpressed reductive enzymes (including glutathione, nitroreductase, azoreductase and DT-diaphrose) ,[3-5] could be useful as triggers for tumor diagnosis and antitumor treatment.[6,7] Among them, NTR switchable fluorophores have received lots of attention due to their exceptional sensitivity.[8-11] The combining of fluorescence recovery together with chemotherapy, photodynamic therapy and radiotherapy[12,13] have achieved obvious development in theranostic platform. However, tumor hypoxia is also known as the "Achilles' heel" of traditional photodynamic therapy (PDT), because severe tumor hypoxia hampers therapeutic outcomes of oxygen-dependent PDT and PDT potentiates hypoxia.

Gene therapy is a promising treatment through silencing abnormally overexpressed gene or compensating defective gene,[14, 15] which has no conflict to the hypoxia condition. It might be a good choice for the NTR triggered theranostic therapy. Especially, visual tracing gene gives intuitive and quantitative evaluation of the dynamic delivery processes at both cellular and tissue levels in a real-time fashion.[16,17] It is generally known that directly labeling genes could influence their biological effect, the probes are usually physically encapsulated or chemically bonded to periphery of the nano-carriers. However, these loading modes for fluorescent nanomaterials often suffer from premature leakage.[18,19] Thus, integrated fluorescent probe boron-dipyrromethene (BODIPY) as the "main" portion has been designed as drug carrier,[20] and PEGylated platinated-BODIPY molecules have been developed to combine chemical, photodynamic and photothermal therapy together for tumor ablation.[21] Our previous work have proved arginine-rich amphiphilic lipopeptides owned excellent gene transfection activity,[22-24] and microenvironment-responsive modification could strongly promote both specificity and efficiency of gene expression.[25,26] While our recent investigations further confirm that dual or multi-responsive triggers in carrier design showed deeper biological understanding of tumor micro-environment, and resulted in high-specific, high-efficient and low-toxic therapy.[27,28] The high GSH concentration (at least 4 fold higher) is one of important characteristics that distinguish tumor tissue/cells from normal tissue/cells. [29-30] Therefore, we intend to utilize the feature of high-concentrated NTR and GSH around tumor and intra-tumor cells simultaneously. Accordingly, NTR-sensitive near-infrared fluorescence molecule was designed as the hydrophobic segment, which would be quenched due to photoinduced electron transfer.[31-33]

We herein developed an NTR and GSH-induced "turn-on" assemblies (RNNS) for gene delivery and targeted imaging with real-time visualization of carrier metabolism (Scheme 1). The carriers possess arginine-rich hydrophilic moiety for efficient gene condensation and cytomembrane penetration, a derivative of cyanine dye in the skeleton structure of amphiphilic molecule as hydrophobic moiety for NTR-sensitive fluorescence imaging, and a disulfide bond as trigger for GSH-responsive cargo release in tumor sites.

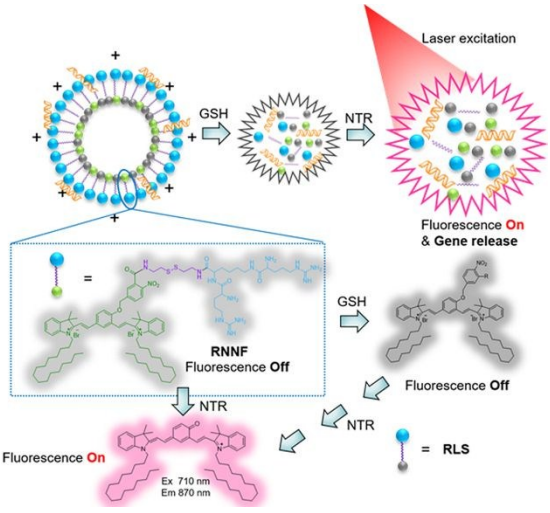

[a]National Engineering Research Center for Biomaterials, Sichuan University, No. 29, Wangjiang Road, Chengdu 610064, P. R. China.
[b] Institute of Regulatory Science for Medical Devices, National Engineering Research Center for Biomaterials, Sichuan University, No. 29, Wangjiang Road, Chengdu 610064, P. R. China.
[c] Johannes Gutenberg-University Mainz, Organic Chemistry, Duesbergweg 10-14, MainZ, DE 55099.
* Corresponding authors: E-mail: nie_yu@scu.edu.cn, xusong2016@scu.edu.cn
†The authors contributed equally to this article.
Electronic Supplementary Information (ESI) available: See DOI: 10.1039/x0xx00000x.

Scheme 1. NTR and GSH responsive nanoplatform for gene delivery and fluorescence imaging.

The synthetic route of targeted molecule RNNF and details were presented in Fig. S1, and the structure characterization of each molecule has been performed through nuclear magnetic resonance spectrum (NMR) and MS (Fig. S2-S13). The amphiphilic molecule RNNF could self-assemble into nano-sized assemblies with Z-Average size of 340 nm and zeta potential of +29 mV. It could be also mixed with another amphiphilic molecule (RLS) synthesized in our previous work[23] with different molar ratios (1/1, 1/2 and 1/3) to obtain smaller assemblies (RNNS, size from 130-185 nm) and better size distribution. The RNNS-3 assemblies (RNNF/RLS, molar ratio= 1/3) showed the minimal size of 136 nm with positive charge (+22 mV) (Table S1). The larger diameter might be owing to both strong hydrophobicity and rigidity of fluorescence molecule (RNNF) during self-assembly.[34-36] While addition of flexible molecule RLS might be conducive to tight integration between molecules, inducing smaller size in process of assembly.[23] The size of all assemblies increased after DNA condensation, and the zeta potential reduced slightly. As a representative, the morphology of RNNS-3 assemblies and RNNS-3/DNA complexes were observed through the transmission electron microscopy (TEM). RNNS-3 assemblies showed a uniform discoid shape, and RNNS-3/DNA complexes revealed a uniform ellipsoidal shape (Fig. 1A and B). The fluorescence spectral characteristic of various molecule and assemblies in organic or aqueous solutions were investigated to detect the on-demand "OFF" and "ON" signals, respectively (Fig. 1C). RNNF had no fluorescence signal in organic solution, even after incubation with GSH. While the spectral peak significantly enhanced in the presence of both NTR and NADH. It indicated specific response of RNNF molecules to NTR with outstanding turn-on effect on fluorescence recovery, which might be beneficial for reducing the background interference.

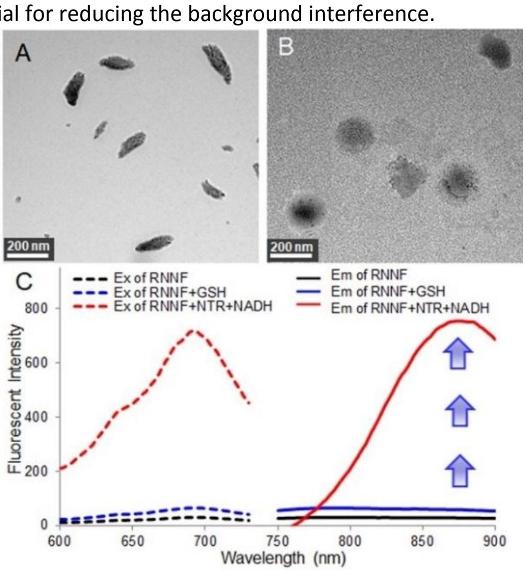

Fig. 1. Characterization of RNNS-3 assemblies and RNNS-3/DNA complexes by TEM and fluorescence spectra of RNNF in various solutions. TEM image of RNNS-3 assemblies (A) and RNNS-3/DNA complexes (B), respectively. (C) Fluorescence spectra of RNNF in various solutions with maximal excitation wavelength (dotted line, Em 870 nm) and emission wavelength (solid line, Ex 690 nm), respectively. Black lines: RNNF in methanol, red lines: RNNF in mixed solution (methanol/water, 1/1, v/v) with 10 mM GSH for 2 h, blue lines: RNNF in mixed solution (methanol/water, 1/1, v/v) with 5 μg/mL NTR and 1 mM NADH for 2 h.

In order to evaluate the selective disassembly response of assemblies, RLS, RNNF, RNNS-1, 2, 3 and 4 were incubated with GSH, NTR or their mixture, respectively. The changes of size and zeta potential were shown in Fig. 2A and S14. RLS and RNNF displayed the most rapid increase on size when incubated with GSH and NTR, respectively. While RNNF/RLS assemblies showed relatively slow responses in the conditions only with GSH or NTR. It might be RNNF partly prevented the degradation of RLS by GSH, and the RLS also disturb the interaction between RNNF and NTR. What's more, noticeable changes of size and zeta potential in all assemblies were shown on condition with both GSH and NTR, revealing the successful disassembly.

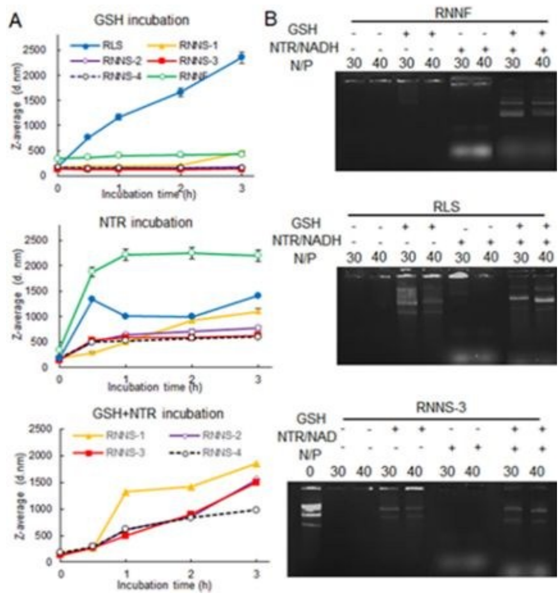

Fig. 2. The selective disassembly response and corresponding gene release of various assemblies in different conditions. (A) The changes of size for various assemblies (RNNF, RLS and RNNS) after incubation with 10 mM GSH, 5 μg/mL NTR and 1 mM NADH, or mixture of GSH and NTR, respectively. Date are presented as means ± SD (n = 5). (B) The gene release ability of different assemblies/DNA complexes in the presence of 10 mM GSH, 5 μg/mL NTR with 1 mM NADH, or mixed GSH and NTR, respectively.

Some research found assemblies with rigid structure could conduce to building tight interaction with cargos and improve the ability of gene condensation.[35,36] Thus, we evaluated gene compaction status in various assemblies with different N/P ratios through gel electrophoresis (Fig. S15) and RNNS-3 was chosen as a representative for the mixed assemblies. It was clear that pDNA could be completely dragged in the loading position by RLS at N/P ratio of 60, by RNNF at N/P ratio of 20 and by RNNS-3 at N/P ratio of 30, respectively. RNNF with relatively rigid structure really showed benefit for the condensation, and addition of it could contribute for gene compaction with lower N/P in the mixed assemblies. Followingly, gene release ability of these assemblies was investigated in the presence of GSH, NTR or their mixture, respectively (Fig. 2B). The images showed that in the presence of either GSH or NTR alone, the release of gene in RNNF, RLS and RNNS assemblies was incomplete. This revealed that fluorescence could recovery in NTR solution but with no gene release (Fig. 1). However, all the

assemblies could completely release gene in the combined action of GSH and NTR.

Although it has been reported that NTR has relatively high content in tumor cells due to the hypoxia environment,[37] seldom relevant data could support this statement.[8-11] Therefore, the content of NTR in tumor cells (HeLa) and non-tumor cells (Human umbilical vein endothelial cells, HUVEC) were detected by Human NTR ELISA Kit, showing certainly higher in Hela cells than that in HUVEC (Fig. S16). In addition, GSH concentration has also been confirmed highly expressed in Hela. [22,38] Followingly, fluorescence recovery of RNNS-3 gene complexes was studied on HeLa with HUVEC as control (Fig. 3A). It was obviously that the fluorescent signal in HeLa was gradually enhanced with the incubation time. While only slight changes were observed in HUVEC. The semi-quantitative evaluation also confirmed these results, showing almost 5-fold difference in intensity (Fig. S17). We could speculate that the fluorescence of RNNS-3 could recovery in the interaction with NTR and GSH in Hela.

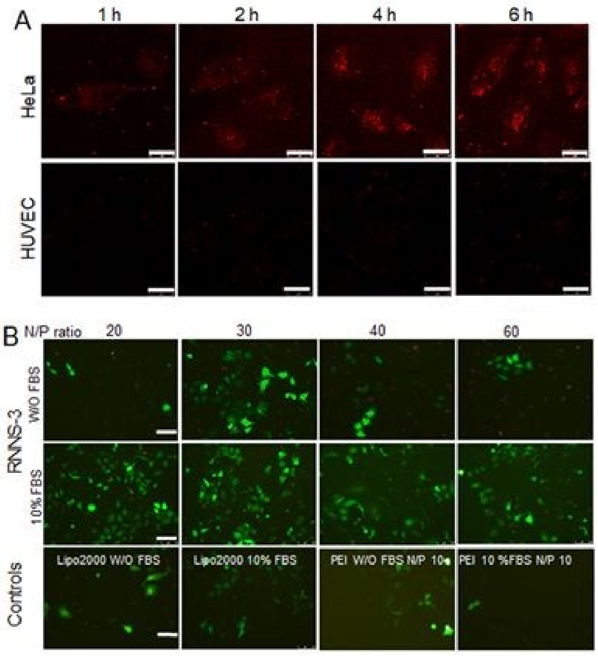

Fig. 3. Fluorescence recovery and *in vitro* gene transfection efficiency of RNNS-3. (A) Fluorescence recovery image of RNNS-3 observed through laser scanning confocal microscope (CLSM). The plasmid DNA were condensed by RNNS-3 assemblies at N/P = 30. HeLa (tumor cells) and HUVEC (non-tumor cells) were incubated with the RNNS-3/DNA complexes for different time (1, 2, 4 and 6 h). The fluorescent signals (red) were observed with 663 nm laser-excitation and 700 ~ 800 nm emission signals. Scale bar= 100 µm. (B) Fluorescence microscopy images of Hela with EGFP transfection for 48 h in the culture medium without or with 10% FBS. pEGFP plasmid DNA were condensed by RNNS-3 assemblies at different N/P ratios (N/P = 20, 30, 40 and 60). Lipofectamine 2000 and PEI (MW = 25000) were acted as control groups. The N/P ratio of PEI/DNA complexes were 10.[22-24] Liposome 2000/DNA complex was 0.2 µL/ 100ng according to the protocol. Scale bar= 100 µm.

In vitro gene transfection activity of these assemblies was also studied on HeLa, and pEGFP plasmid was acted as the model gene (Fig. 3B and S18). More green fluorescent spots were observed from RNNS-3 group compared with PEI or lipofectamine 2000, either in the presence or absence of 10% FBS. On the culture medium with 10 % FBS, the gene transfection activity of these mixed assemblies has decreased in a certain extent, but still far surpassed that in the control groups (Fig. 3B and S18). RNNS-3 assemblies showed the best gene transfection effect at N/P = 30, reaching up to 30-fold higher than commercial reagents (Lipofectamine 2000 and PEI). Flow cytometry data also confirmed RNNS-3 (N/P=30) retained a high gene expression on HeLa cells with 10% serum (Fig. S19). The gene transfection efficiency would be gradually improved with the increase ratio of RNNF. But excessive rigidity would obstruct the interaction between nanocarriers and cell membrane, even hindered the endocytosis and gene release.[39] Meanwhile, the cytotoxicity was another factor that influence the gene transfection effects, which might lead to the poor gene transfection efficiency of RNNS-1 (Fig. S20). The order of cytotoxicity for these assemblies was RNNS-1 > RNNS-2 > RNNS-3 > RNNS-4. Almost no toxicity was observed in RNNS-3 groups on the concentration below 60 µg/mL, which was suitable for *in vitro* and *in vivo* application. According to our previous works, RLS showed very low cytotoxicity.[22-24] We speculated that the cytotoxicity was mainly caused by RNNF. The addition of RLS has significant neutralizing effect on the rigidity of RNNF, thus reducing the cytotoxicity of mixed assemblies. As a result, the RNNS-3 assemblies with part rigid structure and low cytotoxicity have the best performance on gene transfection whether in the condition of culture medium with or without FBS.

In the animal experiment, RNNS-3/pEGFP showed turn-on effect in tumor site (Fig. S21). The near-infrared (NIR) fluorescence could maintained strong until 6 h post-injection, as shown in living mice imaging (Fig. S21A) and ex vivo imaging of the isolated tissues (Fig. S21B). Images also reflected that the indocyanine green (ICG) analogs degraded from RNNS-3 could be metabolized by liver and excreted by kidney.[40] This result confirmed that RNNS-3 could be degraded or metabolize and safe for humans. *In vivo* gene transfection was studied at 48 h post-injection (Fig. 4). Compared with PEI/pEGFP group, the frozen sections of isolated tumors in RNNS-3/pEGFP group showed that considerable green fluorescence corresponded well to the result of NIR channel, indicating that NIR provide the accurate location for gene expression in tumor site.

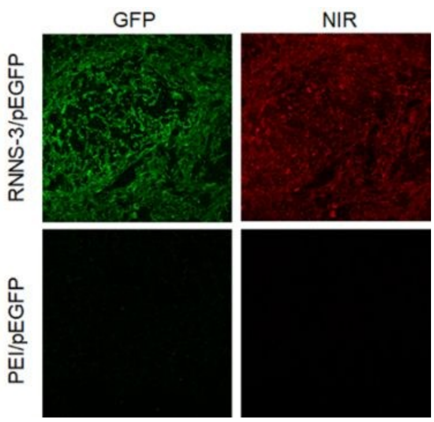

Fig. 4. In vivo green fluorescent protein expression and fluorescent signals in tumors at 48 h after intratumoral injection of RNNS-3/pEGFP (N/P = 30) and PEI/ pEGFP (N/P = 10).

In summary, we designed a kind of amphiphilic lipopeptide molecule RNNF which could be used as theranostic nanoplatform for tumor disease through self-assembly. The mixed assemblies RNNS-3 (RNNF/RLS = 1/3) have minimal size at 136 nm and their fluorescence showed NTR-responsiveness with the maximal emission wavelength at 870 nm. Although RNNF and RLS assemblies have different sensitive responsiveness to NTR and GSH respectively, RNNS-3 assemblies showed good responsiveness to both and good performance on gene condensation and release in the condition of NTR or GSH. Moreover, with low cytotoxicity, RNNS-3 presented the excellent performance on fluorescence recovery and efficient gene transfection both *in vitro* and *in vivo*. Their gene transfection activity was even much better than commercial reagents such as Lipofectamine 2000 and PEI (MW = 25000).

This work was supported by the National Key Research and Development Plan of China (2017YFC1104601), the National Natural Science Foundation of China (NSFC, No. 81873921 and 51903174), Sino-German cooperation group project (GZ1512) and Sichuan Science and Technology Program (2019JDJQ0027).

Conflicts of interest

There are no conflicts to declare.

Notes and references

1. D. Hanahan and R. A. Weinberg, *Cell*, 2011, **144**, 646-674.
2. A. L. Harris, *Nat. Rev. Cancer.*, 2002, **2**, 38-47.
3. Y. Chen and L. Hu, *Med. Res. Rev.*, 2009, **29**, 29-64.
4. M. I. Uddin, S. M. Evans, J. R. Craft, L. J. Marnett, M. J. Uddin and A. Jayagopal, *ACS. Med. Chem. Lett.,* 2015, **6**, 445-449.
5. W. J. Oyen, J. H. Kaanders and J. Bussink, *Q. J. Nucl. Med. Mol. Imaging.*, 2013, **57**, 217-218.
6. L. Zhang, X. Shan, L. Guo, J. Zhang, J. Ge, Q. Jiang and X. Ning, *Analyst*, 2018, **144**, 284-289.
7. D. Ma, C. Huang, J. Zheng, W. Zhou, J. Tang, W. Chen, J. Li and R. Yang, *Anal. Chem.*, 2019, **91**, 1360-1367.
8. J. Zheng, Y. Shen, Z. Xu, Z. Yuan, Y. He, C. Wei, M. Er, J. Yin and H. Chen, *Biosens. Bioelectron.*, 2018, **119**, 141-148.
9. L. Cui, Y. Zhong, W. Zhu, Y. Xu, Q. Du, X. Wang, X. Qian and Y. Xiao, *Org. Lett.*, 2011, **13**, 928-931.
10. H. C. Huang, K. L. Wang, S. T. Huang, H. Y. Lin and C. M. Lin, *Biosens. Bioelectron.*, 2011, **26**, 3511-3516.
11. M. Srinivasarao, C. V. Galliford and P. S. Low, *Nat. Rev. Drug Discov.*, 2015, **14**, 203-219.
12. Q. M. Zhang, C. Jin, J. H. Yu and W. Lu, *Acs Omega*, 2018, **3**, 8813-8818.
13. Z. Liu, F. Song, W. Shi, G. Gurzadyan, H. Yin, B. Song, R. Liang and X. Peng, *ACS Appl. Mater. Interfaces*., 2019, **11**, 15426-15435.
14. P. Zarogoulidis, E. Chatzaki, W. Hohenforst-Schmidt, E. P. Goldberg, G. Galaktidou, T. Kontakiotis, N. Karamanos and K. Zarogoulidis, *Cancer. Gene. Ther.*, 2012, **19**, 593-600.
15. X. M. Anguela and K. A. High, *Annu. Rev. Med.*, 2019, **70**, 273-288.
16. N. Boehnke, S. Correa, L. Hao, W. Wang, J. P. Straehla, S. N. Bhatia and P. Hammond, *Angew. Chemie. Int. Ed.*, 2020, **132**, 2936-2936.
17. X. He, Q. Luo, J. Zhang, P. Chen, H. J. Wang, K. Luo and X. Q. Yu, *Nanoscale*, 2019, **11**, 12973-12982.
18. J. Croissant and J. I. Zink, *J. Am. Chem. Soc.*, 2012, **134**, 7628-7631.
19. D. Gyawali, S. Y. Zhou, R. T. Tran, Y. Zhang, C. Liu, X. C. Bai and J. Yang, *Adv. Healthc. Mater.*, 2014, **3**, 182-186.
20. X. G. Liu, M. Wu, Q. L. Hu, H. Z. Bai, S. Q. Zhang, Y. Q. Shen, G. P. Tang and Y. Ping, *ACS Nano*, 2016, **10**, 11385-11396.
21. Z. Q. Guo, Y. L. Zou, H. He, J. M. Rao, S. S. Ji, X. N. Cui, H. T. Ke, Y. B. Deng, H. Yang, C. Y. Chen, Y. L. Zhao and H. B. Chen, *Adv. Mater.*, 2016, **28**, 10155-10164.
22. X. Chen, J. Yang, H. Liang, Q. Jiang, B. Ke and Y. Nie, *J. Mater. Chem. B.*, 2017, 5, 1482-1497
23. H. Liang, A. Hu, X. Chen, R. Jin, K. Wang, B. Ke and Y. Nie, *J. Mater. Chem. B.*, 2019, 7, 915-926.
24. X. Xu, Q. Jiang, X. Zhang, Y. Nie, Z. Zhang, Y. Li, G. Cheng and Z. Gu, *J. Mater. Chem. B.*, 2015, **3**, 7006--7010.
25. Y. Y. He, G. Cheng, L. Xie, Y. Nie, B. He and Z. W. Gu, *Biomaterials*, 2013, **34**, 1235-1245.
26. Y. Y. He, Y. Nie, L. Xie, H. M. Song and Z. W. Gu, *Biomaterials*, 2014, **35**, 1657-1666.
27. X. Jia, Y. Zhang, Y. Zou, Y. Wang, D. Niu, Q. He, Z. Huang, W. Zhu, H. Tian, J. Shi and Y. Li, *Adv. Mater.*, 2018, **30**, e1704490.
28. W. Tang, W. Fan, Z. Wang, W. Zhang, S. Zhou, Y. Liu, Z. Yang, E. Shao, G. Zhang, O. Jacobson, L. Shan, R. Tian, S. Cheng, L. Lin, Y. Dai, Z. Shen, G. Niu, J. Xie and X. Chen, *ACS Nano*, 2018, **12**, 12269-12283.
29. P. Kuppusamy, H. Li, G. Ilangovan, A. J. Cardounel, J. L. Zweier, K. Yamada, M. C. Krishna and J. B. Mitchell, *Cancer Res.*, 2002, **62**, 307–312.
30. R. Mo and Z. Gu, *Mater. Today*, 2016, **19**, 274–283.
31. A. Chevalier, Y. Zhang, O. M. Khdour, J. B. Kaye and S. M. Hecht, *J. Am. Chem. Soc.*, 2016, **138**, 12009-12012.
32. S. Y. Lim, K. H. Hong, D. I. Kim, H. Kwon and H. J. Kim, *J. Am. Chem. Soc.*, 2014, **136**, 7018-7025.
33. L. Feng, R. Xie, C. Wang, S. Gai, F. He, D. Yang, P. Yang and J. Lin, *ACS nano*, 2018, **12**, 11000-11012.
34. M. Piest and J. F. J. Engbersen, *J. Control. Release*, 2010, **148**, 83-90.
35. B. Wang, R. M. Zhao, J. Zhang, Y. H. Liu, Z. Huang, Q. Y. Yu and X. Q. Yu, *Eur. J. Med. Chem.*, 2017, **136**, 585-595.
36. S. Raffy and J. Teissié, *Biophys. J.*, 1999, **76**, 2072-2080.
37. Z. Zhou, J. Song, L. Nie and X. Chen, *Chem. Soc. Rev.*, 2016, **45**, 6597-6626.
38. L. Y. Niu, Y. S. Guan, Y. Z. Chen, L. Z. Wu, C. H. Tung and Q. Z. Yang, *J. Am. Chem. Soc.*, 2012, **134**, 18928-18931.
39. C. L. Grigsby and K. W. Leong, *J. R. Soc. Interface*, 2010, **7**, 67-82.
40. J. Zhao, Z. Wan, C. Zhou, Q. Yang, J. Dong, X. Song and T. Gong, *Pharm. Res*, 2018, **35**, 196

View Article Online
DOI: 10.1039/C9CC10071G

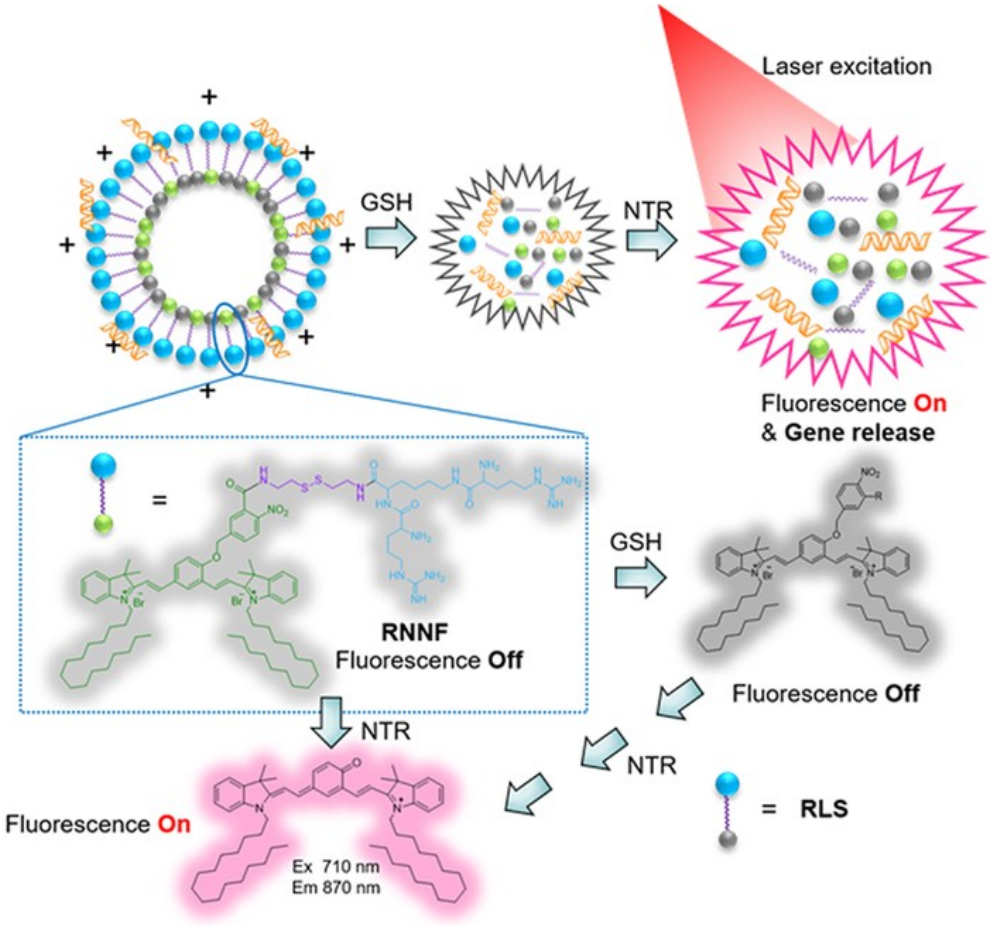

59x55mm (300 x 300 DPI)